# Two-photon absorption laser induced fluorescence measurements of absolute neutral deuterium density, temperature, and bulk flow in Proto-MPEX

Cite as: Phys. Plasmas **28**, 082501 (2021); doi: 10.1063/5.0054734 Submitted: 21 April 2021 · Accepted: 12 July 2021 · Published Online: 2 August 2021







Thomas E. Steinberger, <sup>1,a)</sup> D Jacob W. McLaughlin, <sup>2</sup> Theodore M. Biewer, <sup>3,4</sup> D Juan F. Caneses, <sup>3</sup> D and Earl E. Scime D

#### **AFFILIATIONS**

- <sup>1</sup>Department of Physics and Astronomy, West Virginia University, Morgantown, West Virginia 26506, USA
- <sup>2</sup>Department of Physics and Astronomy, University of Iowa, Iowa City, Iowa 52242, USA
- <sup>3</sup>Oak Ridge National Laboratory, Oak Ridge, Tennessee 37831, USA
- <sup>4</sup>Bredesen Center, University of Tennessee, Knoxville, Tennessee 37996, USA

#### **ABSTRACT**

Neutral particle control is critical for fusion fueling and confinement. Neutral diagnostics for fusion-relevant plasmas are commonly restricted to line-integrated or  $ex\ situ$  methods. A non-perturbative, two-photon absorption laser induced fluorescence (TALIF) diagnostic is implemented on the Prototype Material Plasma Exposure eXperiment (Proto-MPEX) to probe neutral atomic deuterium in a fusion-relevant plasma at 1 cm intervals along the radius of the vacuum vessel. The diagnostic is situated  $\sim$ 20 m from the vacuum vessel, and a signal is collected along the laser injection axis, requiring only one line-of-sight. TALIF measurements are absolutely calibrated using xenon and krypton. Absolute atomic densities derived from xenon calibration are compared to absolute atomic densities derived from krypton calibration. Here, preliminary measurements of absolute atomic deuterium density, temperature, and local bulk flow dependence on radial location and input power in Proto-MPEX are presented. Neutral atomic deuterium velocity distribution functions are measured throughout a one-second plasma pulse with a time resolution of 250 ms.

Published under an exclusive license by AIP Publishing. https://doi.org/10.1063/5.0054734

#### I. INTRODUCTION

High density, magnetically confined fusion plasmas rely on several neutral processes to sustain favorable confinement conditions. Neutral recycling from reactor walls and the divertor supply fuel to the plasma, ion-neutral charge exchange both carries energy away from the core of the fusion plasma and is responsible for heating and momentum input when neutral beams are injected into fusion plasmas,<sup>2,3</sup> and neutral density in the edge of fusion devices has been identified as a critical parameter for confinement mode transitions.<sup>4,5</sup> Control of these processes requires detailed knowledge of the neutral density, the neutral velocity distribution, and the neutral temperature.<sup>6</sup> These parameters are frequently estimated with neutral simulation codes such as SOLPS.7 However, Hubbard emphasizes that predictions of the fusion core from simulation are extremely sensitive to the initial input parameters for neutral particles in the edge of fusion devices.8 Therefore, it is evermore necessary to validate predictions from simulations with spatially localized non-perturbative experimental measurements of neutrals. Neutral dynamics are commonly studied by observing neutral emission, but these techniques are line-integrated, and additional measurements and analysis are needed to recover one-dimensional spatially localized information.

Laser induced fluorescence (LIF) has become a standard technique of investigating ions and neutrals non-perturbatively since it was first introduced by Stern and Johnson. Mertens and Silz used LIF to measure neutral densities in the edge of TEXTOR 94.6 However, these measurements lacked spatial resolution and required a laser that produced poorly transmitted 102 nm photons. A similar technique, two-photon absorption laser induced fluorescence (TALIF), uses easier to generate photons (205 – 225 nm) to probe ground state atoms in a variety of plasmas. Heliotron-E plasma device with a spatial resolution of tens of mm and used a global predetermined calibration technique to determine absolute neutral density that did not take into account changes in laser or machine

<sup>&</sup>lt;sup>a)</sup>Author to whom correspondence should be addressed: testeinberger@mail.wvu.edu

performance.<sup>15</sup> Elliott *et al.* used TALIF to investigate neutral atomic deuterium densities and temperature on the HIT-SI3 experiment<sup>16</sup> and identified a novel xenon calibration scheme for deuterium TALIF measurements.<sup>17</sup>

Here, TALIF is employed to make *in situ*, spatially and temporally resolved measurements of neutral atomic deuterium velocity distribution functions (NVDFs) in the Prototype Plasma Material Exposure eXperiment (Proto-MPEX). Measurements of atomic deuterium are absolutely calibrated with xenon using the scheme identified in Ref. 17 and with krypton. Absolute densities from both calibration gases are compared. The TALIF measurements presented here are performed with a confocal injection and collection optical configuration that requires one point of optical access, an attractive feature for fusion devices.

The remainder of this work is structured as follows. In Sec. II, a description of the TALIF system and an overview of Proto-MPEX are given. The details of TALIF are outlined in Sec. III. Results are presented in Sec. IV. Finally, discussion of the results and conclusions are covered in Sec. V.

# II. EXPERIMENTAL CONFIGURATION A. TALIF laser system, collection apparatus, and electronics

A two-laser system is used in this work to produce 205 nm photons. A Spectra Physics Quanta Ray Pro 270 pulsed Nd:YAG laser generates a maximum of 600 mJ/pls of 532 nm light and pumps a Sirah Cobra Stretch dye laser equipped with a third harmonic tripling stage. The 532 nm light is frequency converted to produce  $\sim\!130$  mJ/pls of 615 nm light, referred to as the fundamental, using a rhodamine 610 and rhodamine 640 solution. The fundamental is frequency tripled to produce a maximum of 4 mJ/pls ( mJ/pls typical) of 205 nm light over 8 ns pulses at a repetition rate of 20 Hz.

The laser wavelength is changed at the dye stage of the laser by adjusting two 2400 groove/mm gratings. The rhodamine dye solution has a lasing wavelength range of 609 - 640 nm with peak power efficiency at 615 nm. Excess light from the gratings is captured by a  $\varnothing 5\,\mu m$  core single mode fiber coupled to an Ångstrom/High Finesse WS7 wavelength meter for real-time monitoring of the laser

wavelength, linewidth, and power at the dye conversion stage. An energy-per-pulse conversion curve for laser energies measured at the dye conversion stage compared to UV energies delivered to the vacuum vessel is created for wavelength ranges needed for each TALIF scheme used in this work. This provides an estimate of the energy-per-pulse of UV light at the measurement location during TALIF measurements.

UV light is delivered to Proto-MPEX from a distance of nearly 20 m away. This distance is necessary to keep the laser and laser electronics situated in a low electromagnetic interference environment. Laser emission is free-space aligned to a set of vertically-oriented, confocal optics referred to as the confocal apparatus [Fig. 1(b)]. The confocal apparatus used here is of the same design implemented in Ref. 16. The confocal apparatus provides the ability to inject laser light and collect TALIF signal along the same line-of-sight. A key feature of the confocal apparatus is a mirror mounted at 45° with a 12 mm hole drilled through the center. The injected light passes through the hole in the mirror and is focused to submillimeter scales by a Ø50.8 mm, 150 mm focal length, Ca<sub>2</sub>F objective lens. The TALIF signal is collected by the same lens, is directed through a second Ø50.8 mm lens by the obliquely mounted mirror, and is focused into a  $\emptyset$ 600  $\mu$ m core multimode fiber. The focal waist of the collection volume of the confocal apparatus is  $\leq 5$  mm in diameter and has a depth-of-field that is on similar length scales. Therefore, a conservative upper spatial resolution limit is contained by a  $5 \times 5 \times 5$  mm<sup>3</sup> volume. The confocal apparatus is fastened to a remotely controlled motion stage that allows the focus of the injected laser light to be scanned vertically through the plasma column for measurements at different radial locations. Collected light is filtered using two 1 nm wide bandpass filters centered at 656 nm, and the TALIF signal is amplified by a Hamamatsu H11526-20-NF photomultiplier tube. The PMT output pulse is shaped and further amplified by a Hamamatsu C11184 amplifier. The amplified signal is monitored and recorded using a Stanford Research Systems SR250 Gated Integrator and Box Car Averager. The boxcar averager is triggered at twice the frequency of the laser, i.e., 40 Hz, for active background subtraction of the collected signal. Signal and wavelength measurements are digitized and stored on a standalone computer with an internal National Instruments data acquisition card.

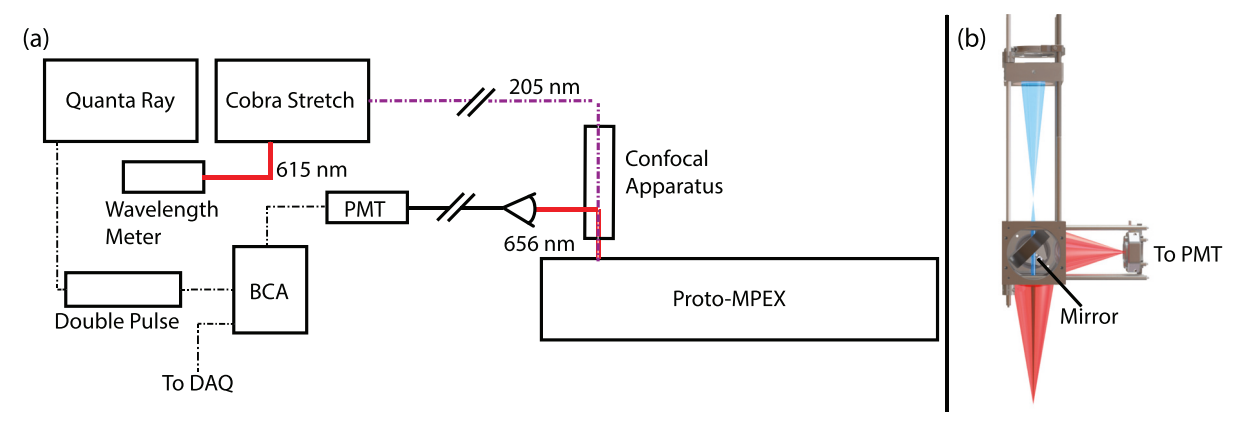


**FIG. 1.** (a) Cartoon of experimental layout. Photomultiplier tube is abbreviated as PMT, double pulse is a double pulse generator, and the boxcar averager is abbreviated as BCA. (b) Rendered image of the confocal apparatus. Injected light is compressed and collimated before passing through the mirror mounted at 45o. Laser light is injected and signal is collected along the same axis. Signal is reflected off the oblique mirror and is focused into a fiber that is coupled to the detecting electronics.

Figure 1 shows a (a) simple cartoon of the experimental configuration and (b) a rendered image of the confocal apparatus.

### B. Prototype material plasma exposure experiment

Proto-MPEX is a linear helicon device constructed at Oak Ridge National Laboratory. 18,19 The configuration of Proto-MPEX is described as it was at the time of these experiments. Figure 2 shows a side-on rendered view of the vacuum vessel with select features annotated. At the time of these experiments, a maximum of 330 kW of installed power was able to be sourced to Proto-MPEX in the form of rf power modulated at 13.56 MHz (200 kW), electron-cyclotron heating (100 kW at 28 GHz), and ion-cyclotron heating (30 kW at 6-9 MHz). However, typical injected powers are much less than the installed power, and auxiliary heating in the form of ion- and electroncyclotron heating was not used for the measurements presented here. Thirteen electromagnet coils (M1–M13), repurposed from the ELMO Bumpy Torus,<sup>20</sup> are placed along the length of Proto-MPEX, and sets of magnets are controlled separately to create a user defined magnetic field profile. From left to right in Fig. 2, Proto-MPEX begins with a large stainless steel dump chamber. The dump chamber is coupled to standard 15.2 cm diameter stainless steel vacuum components that total approximately 1.5 m in length with several vacuum flange ports for diagnostic access. Electromagnets 1-5 surround this section of Proto-MPEX. TALIF measurements are performed between magnets 1 and 2. A water-cooled, double-helix, quarter-turn, m = +1 copper antenna located between magnets 3 and 4 is used to generate and maintain a deuterium plasma pulse. A large rectangular central diagnostic chamber is located between magnets 6 and 7. The inner diameter of the electromagnets forms the vacuum boundary from magnet 5 to magnet 9. An electron-cyclotron auxiliary heating port is located between magnets 8 and 9. Magnets 10 and 11 are ex-vacuum to facilitate the placement of a second antenna for ion-cyclotron auxiliary heating. Magnets 12 and 13 form the vacuum boundary. A boundary plate, referred to as the target, is inserted between magnets 12 and 13.

A total of four turbo-molecular drag pumps that combine for a pumping rate of  $6450\,l/s$  maintain a base pressure of  $\sim 10^{-6}$  Torr in Proto-MPEX. Base and operating pressure are monitored by four MKS Instrument 627 Baratron pressure gauges one each located between magnets 2 and 3, at the central chamber, between magnets 7 and 8, and between magnets 12 and 13, respectively. For this work, the pressure gauge located between magnets 2 and 3 was referenced as it provides the closest measurements of pressure for TALIF experiments. Gas is injected through a nozzle located between magnets 1 and 2 and through two gas rings, located between magnets 2 and 3 and magnets

4 and 5. The gas ring between magnets 4 and 5 was not used for the measurements presented here. Gas flow is controlled using calibrated, fast-acting PV-10 piezo valves, and gas flows of 10 standard liters per minute (SLM) are achievable. Gas flows greater than 2.5 SLM were used for this work, which is greater than maximum gas flows for typical Proto-MPEX experiments.

Standard Proto-MPEX operation is significantly different from the operational mode of Proto-MPEX for the measurements presented here. Typically, Proto-MPEX produces 0.5 s long plasma pulses with rf injection powers of  $\sim\!100-150$  kW. Gas flows of  $\leq\!2.5$  SLM are used to maintain a constant operating pressure at the helicon of  $\sim\!2.5$  mTorr. However, for this work, the plasma pulse length was increased to one second with injected rf powers  $P_{\rm rf} \leq 60$  kW. Gas flows much greater than 2.5 SLM create a constantly increasing operating pressure from  $\sim\!10-150$  mTorr at the helicon over the entirety of a plasma pulse. The TALIF signal outside this modified operational regime of Proto-MPEX was not observed. At higher input rf power, the helicon is more effective at ionizing the available neutral gas, resulting in a lower neutral population for TALIF.

### III. TWO-PHOTON LASER INDUCED FLUORESCENCE

LIF is a spatially localized, non-perturbative, spectroscopic technique that uses laser emission to optically excite electrons from one state to a higher energy state. Fluorescence intensity from the excited state to a lower energy state is measured to construct a velocity distribution function (VDF). In LIF, a single photon provides the exact energy to excite an electron from a metastable state to an excited state in a neutral particle or ion. However, metastable states are not always directly indicative of bulk population or are not readily available in plasmas. The ability to measure particles directly from a ground state is ideal for measuring the absolute state density. Measuring ground state transitions requires energetic photons at wavelengths that are not readily transmittable through standard vacuum components and optics, i.e., 10-150 nm. For this reason, neutrals are probed with TALIF in this work. For the TALIF measurements here, two identical ultraviolet photons are absorbed simultaneously, each providing half the energy to excite the ground state transition. Integrated TALIF signal is well described by

$$I_{LIF} = n \frac{\Omega}{4\pi} \eta T G_{TP} \sigma_{TP}^{(2)} \left(\frac{E}{h\nu}\right)^2 g a, \tag{1}$$

where  $I_{LIF}$  is the integrated signal (photons s m), n is the density of the interrogated species (m<sup>-3</sup>),  $\Omega/4\pi$  is the solid angle of collection normalized by the solid angle of a sphere,  $\eta$  is the unitless quantum

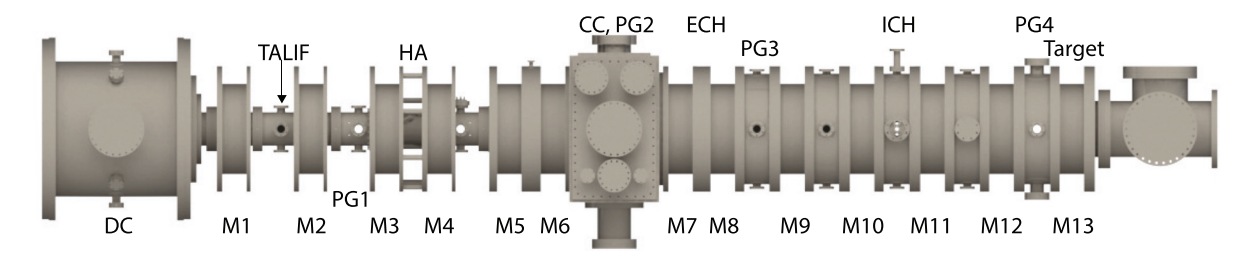


FIG. 2. Rendered image of Proto-MPEX. Abbreviations: Dump chamber (DC), magnets 1–13 (M1–M13), TALIF measurement location (TALIF), pressure gauges 1–4 (PG1–PG4), helicon antenna (HA), electron-cyclotron auxiliary heating location (ECH), ion-cyclotron auxiliary heating location (ICH), and location of target plate (Target).

efficiency of the photodetector at the fluorescence wavelength, T is the transmission of optical components,  $G_{TP}$  is a statistical factor<sup>21</sup> that arises from the nature of an electron absorbing two photons simultaneously and has a value of 2,  $\sigma^{(2)}_{TP}$  is the two-photon absorption cross section (m<sup>4</sup> s photons<sup>-1</sup>), E is the laser energy per pulse (J/pls),  $h\nu$  is the energy per photon (J/photon), g is the gain of the detecting system for the applied voltage on the photodetector, and a is the branching ratio for the fluorescence transition.<sup>13</sup> The two-photon cross section is many orders of magnitude smaller than a single photon absorption cross section, and as a result, most TALIF systems employ a short pulse, (i.e.,  $\Delta t_{\text{pulse}} \lesssim 10$  ns) high intensity laser.

Particle motion, either through random thermal motion or bulk particle velocity, shifts the required transition frequency by the Doppler effect

$$v = \frac{f - f_{\circ}}{f_{\circ}} c = (f - f_{\circ})\lambda_{\circ}, \tag{2}$$

where v is the particle velocity, f is the lab frame absorption frequency,  $f_{\circ}$  ( $\lambda_{\circ}$ ) is the rest frame absorption frequency (wavelength), and c is the speed of light. Sweeping the laser frequency through an absorption profile, the NVDF is constructed using Eq. (2). Neutral temperature, local bulk flow, and relative density are determined from the NVDF. Additionally, if the TALIF measurement is calibrated with a noble gas, then the absolute neutral density is measurable. For this work, atomic deuterium measurements are absolutely calibrated using krypton<sup>12</sup> and xenon using the TALIF scheme first proposed by Elliott et al. 17 Atomic densities derived from both calibration methods are compared. Figure 3 shows a partial Grotrian diagram for each of the species investigated in this work: atomic deuterium, xenon, and krypton. Deuterium and krypton have similar excitation wavelengths, but very different fluorescent wavelengths. The difference in fluorescence wavelength between deuterium and krypton sometimes requires optical realignment between target and calibration measurements. An opposite relation exists between deuterium and xenon, i.e., the excitation wavelength for deuterium is very different from xenon, but the fluorescent wavelengths are nearly identical. The similarity of the deuterium and xenon fluorescent wavelengths eliminates the need for optical realignment between target and calibration measurements.

Absolute calibration of atomic deuterium using a noble gas requires two independent TALIF measurements: one in deuterium and another in the calibration gas. Equation (1) is normalized to the known quantities that are unique to each gas, i.e., quantum efficiency and gain of the detector, laser energy squared, and the branching ratio of the fluorescence transition. The absolute density of atomic deuterium is calculated by taking the ratio of the two normalized integrated signals for deuterium and the calibration gas. Quantities that are common to both gases in Eq. (1) are eliminated in the ratio, and the absolute atomic density of deuterium is solved for if the local pressure of the calibration gas and the relative cross section between atomic deuterium and calibration gas are known. Niemi et al.<sup>22</sup> determined the relative cross section between krypton and atomic deuterium to be  $\sigma_{\rm Kr}/\sigma_{\rm D}=0.62$ . Elliott et al. 17 measured the relative calibration factor between xenon and atomic deuterium to be  $\sigma_{
m Xe}/\sigma_{
m D}=0.024.$  For the absolute densities reported here, the calibration gas densities are based on the measured pressure at the TALIF measurement location.

#### **IV. RESULTS**

NVDFs are constructed from a series of consecutive one second long Proto-MPEX plasma pulses. During this time, 20 laser pulses are recorded, and the laser wavelength is fixed for the entirety of a single plasma pulse. Ten plasma pulses, i.e., ten unique wavelengths, are needed to measure a single deuterium NVDF. Every five laser pulses are averaged over to measure the time evolution of deuterium NVDFs with a resolution of 250 ms. In general, little or no signal is observed for early times in the plasma pulse. Lack of signal persists to later times in the plasma pulse for larger injected rf powers. Atomic deuterium NVDFs are measured for injected rf powers between 30 and 60 kW and for radial locations of r=0,1,2,6, and 7 cm. Measurements for r=3,4, and 5 cm were inaccessible due to a physical obstruction that prevented the confocal optics from being placed at the appropriate distance from the measurement location.

## A. rf Power variation

Figure 4 shows the atomic deuterium NVDF evolution throughout the plasma pulse for injected rf powers of (a) 60, (b) 50, (c) 40, and (d) 30 kW. When available, atomic densities derived from krypton and

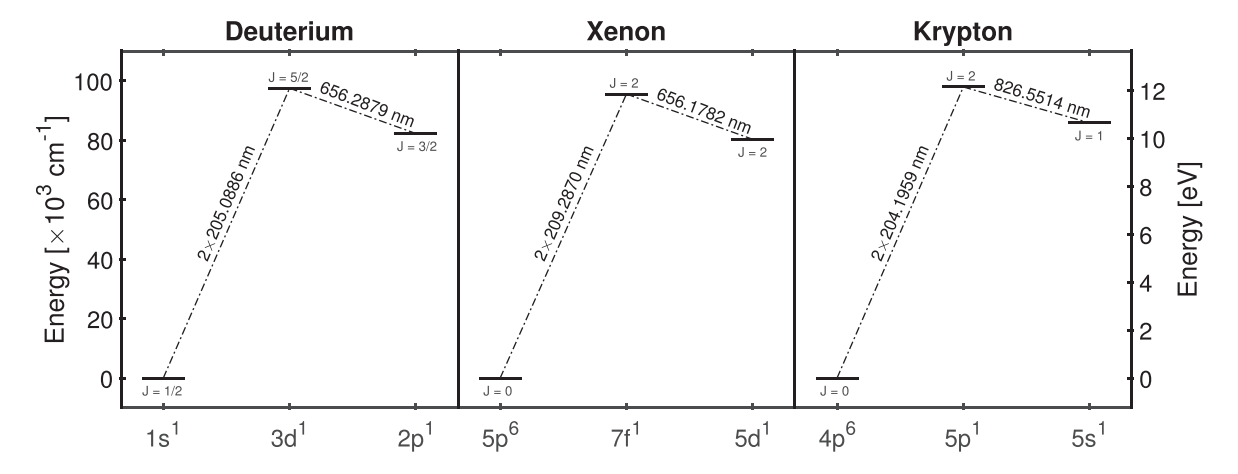
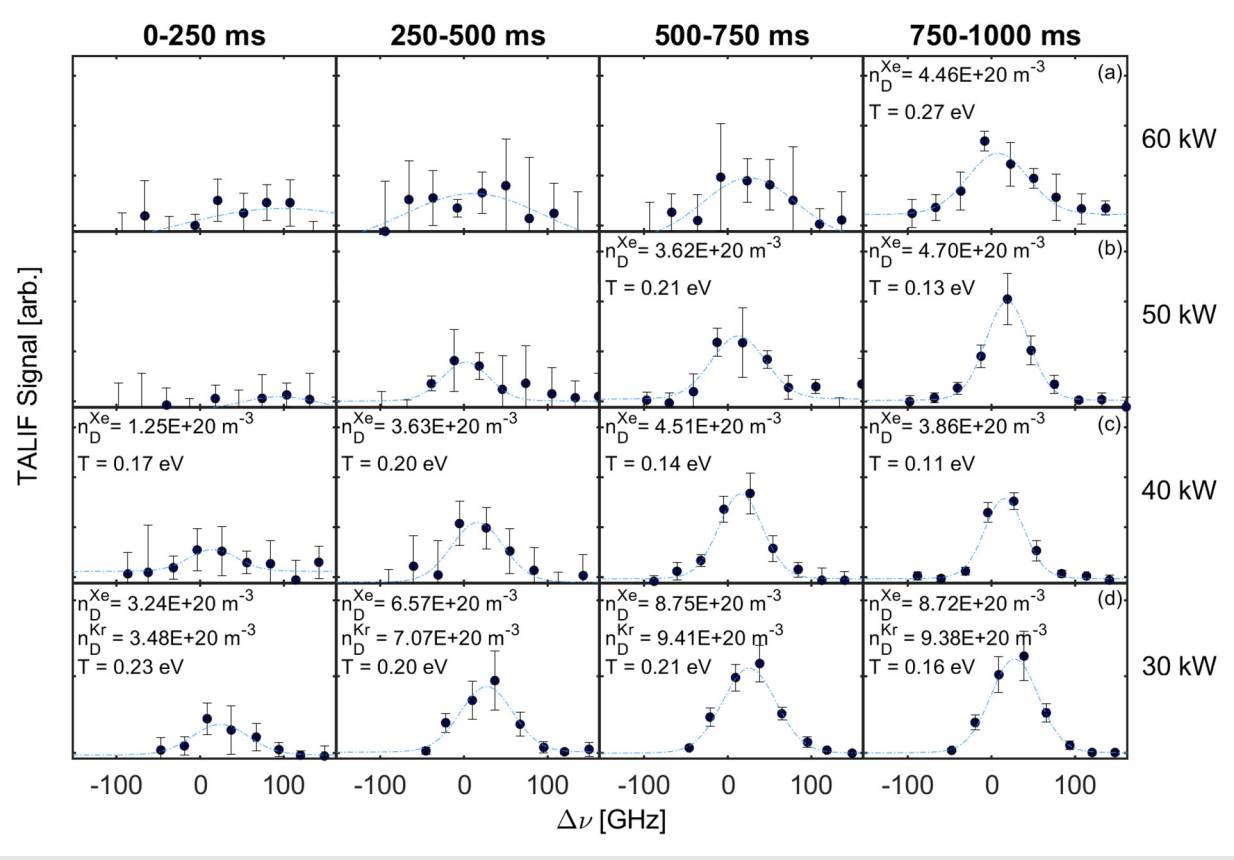


FIG. 3. Partial Grotrian diagram for atomic deuterium, xenon, and krypton schemes used in this work. Atomic deuterium is the target species. Xenon and krypton are used as calibration gases.



**FIG. 4.** Deuterium NVDF evolution over the plasma pulse for (a)  $P_{\rm rf} = 60$  kW, (b)  $P_{\rm rf} = 50$  kW, (c)  $P_{\rm rf} = 40$  kW, and (d)  $P_{\rm rf} = 30$  kW. Absolute atomic density and temperature are shown for every acceptable fit to the data. Lower powers produce sufficient signal for all times during the plasma pulse, whereas only later times exhibit discernible signal for higher powers. Comparison between xenon and krypton calibrated shots is shown where available.

xenon are compared. Derived quantities are shown only for time frames with discernible signal. The TALIF signal intensity generally increases throughout the plasma pulse. This is expected since the pressure increases throughout the plasma pulse. The error bars represent the standard deviation of the signal at each wavelength. Greater variation is seen for earlier times in the plasma pulse or for greater rf injected powers when the discernible signal is poor. A best fit to a Voigt line shape is shown by the light blue dashed line. These data were taken at  $r=2\,\mathrm{cm}$  relative to the mechanical axis.

Neutral atomic deuterium absolute density, temperature, and local bulk flow dependencies on injected rf power are shown in Figs. 5, 6, and 7, respectively. The upper plot in Fig. 5 shows absolute atomic density as a function of injected rf power from 30 to 60 kW for 250 ms intervals throughout the plasma pulse. Atomic densities derived from krypton are shown by light blue open circles, and atomic densities derived from xenon are shown in dark blue solid circles. The lower plot in Fig. 5 shows the average evolution of the total operating pressure (i.e., mixture of atomic and molecular neutral deuterium) over the plasma pulse for each injected rf power. Absolute atomic deuterium densities are nominally measured to be on the order of  $10^{20} \mathrm{m}^{-3}$ . For  $P_{\rm rf} = 30$  kW, deuterium lineshapes were absolutely calibrated with xenon and krypton. Absolute densities calculated from both calibration gases are in excellent agreement despite significantly worse

signal-to-noise (SNR) for the xenon calibration measurements. Measured neutral atomic density shows little dependence on injected rf power. A slight increase in calculated neutral density is observed over the plasma pulse and is consistent with rising gas pressure.

Neutral atomic deuterium temperature, similar to absolute atomic deuterium density, shows little dependence on injected rf power. Measured neutral temperatures are measured to be  $\sim\!0.2$  eV, much less than the expected Frank-Condon neutral temperature of  $\sim\!2$  eV.  $^{23}$  Comparable neutral temperatures were observed by Galante et al. in similar helicon plasmas.  $^{24}$  The suspected reason for the significantly lower neutral temperature is that when no heating mechanisms are present for neutral particles, they tend to rapidly relax to the wall temperature, i.e.,  $T_{\rm neut} \ll 2$  eV. Neutral temperatures decrease over the plasma pulse. This is expected since the gas pressure is rapidly increasing over the plasma pulse. As the gas pressure increases, the plasma becomes more collisional and starts to terminate, both processes facilitate a cooling of the neutrals.

Measured neutral velocity as a function of injected rf power is shown in Fig. 7. Neutral atoms are measured to be flowing radially inward at r=2 cm for all injected powers. The neutral particle motion for each injected rf power is steady over the plasma pulse. Neutral velocity decreases with increasing injected rf power, and peak neutral flows are as large as  $\sim 3$  km/s.

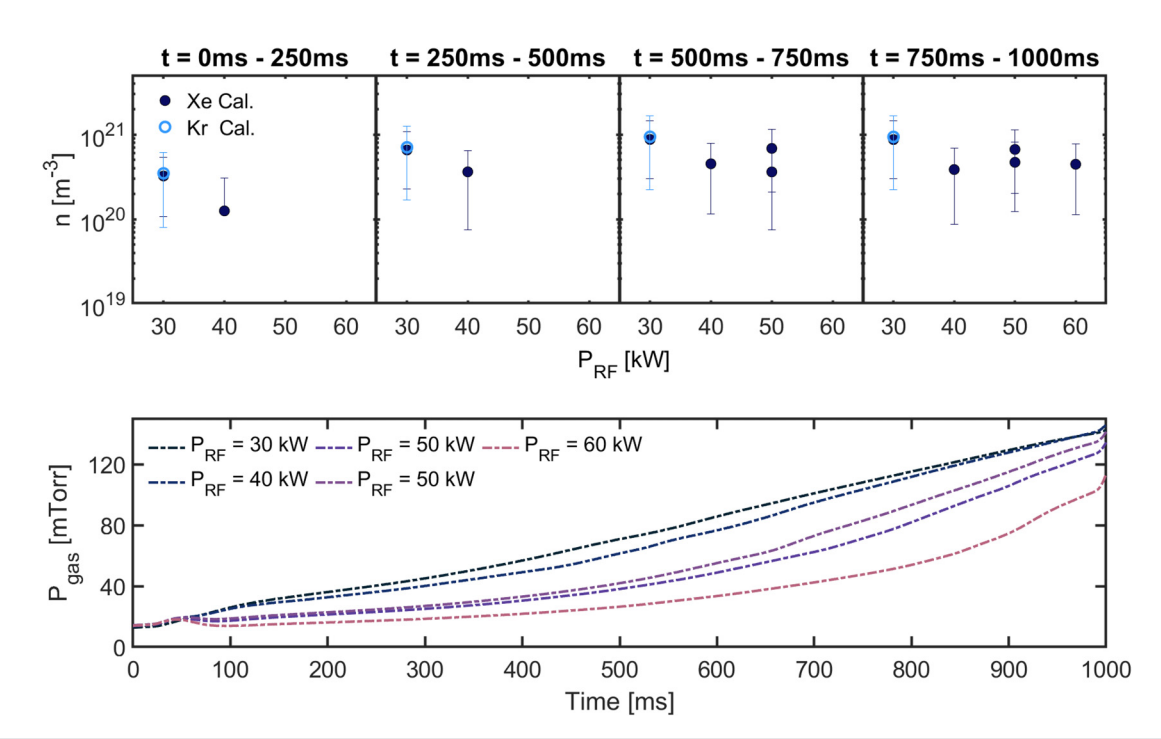


**FIG. 5.** (Upper plot) Evolution of neutral atomic density throughout the plasma pulse as a function of  $P_{\rm rf}$ . Density was calibrated with both xenon and krypton for  $P_{\rm rf}=30$  kW. Atomic density values derived from krypton are shown in light blue open circles, and atomic density values derived from xenon are shown with dark blue solid circles. (Lower plot) Total neutral pressure evolution over the duration of the plasma pulse.

#### **B.** Radial variation

Neutral atomic deuterium TALIF signal intensity evolution over the Proto-MPEX pulse for different radial locations for 250 ms time intervals is displayed in Fig. 8. The confocal optical arrangement was scanned vertically through the plasma column to obtain measurements at different radial locations. Radial measurements were obtained at  $P_{\rm rf}=30$  kW. Discernible TALIF signal is observed at all times throughout the plasma pulse, though signal-to-noise increases for later times in the pulse. Additionally, absolute atomic densities were derived from xenon and krypton for all radial measurements. Atomic deuterium lineshapes are measured from ten Proto-MPEX pulses as a

function of radial location. The blue dashed line indicates a best fit to a Voigt profile. A clear increase in atomic deuterium signal intensity throughout the plasma pulse is observed.

Neutral atomic deuterium density as a function of radial distance is shown in the upper panel of Fig. 9. Absolute atomic densities derived from krypton are shown by the light blue open circles, and atomic densities derived from xenon are shown in the dark blue solid circles. The lower panel of Fig. 9 shows the average evolution of the total neutral pressure (i.e., mixture of atomic and molecular neutral deuterium) for each set of radial measurements, and five total pressure traces are displayed. At the operating parameters of Proto-MPEX during these experiments, the neutral atomic density profile is essentially

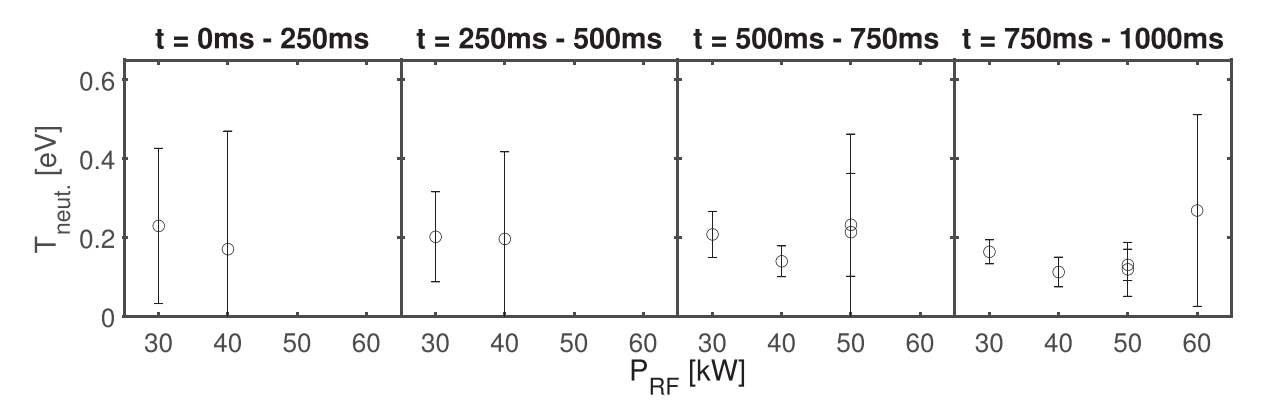


FIG. 6. Neutral deuterium temperature as a function of operating power. Temperatures derived from fits with sufficient signal are shown. A general decrease in temperature for later times throughout the pulse is observed due to the lack of the persistence of the plasma for higher pressures and later times.

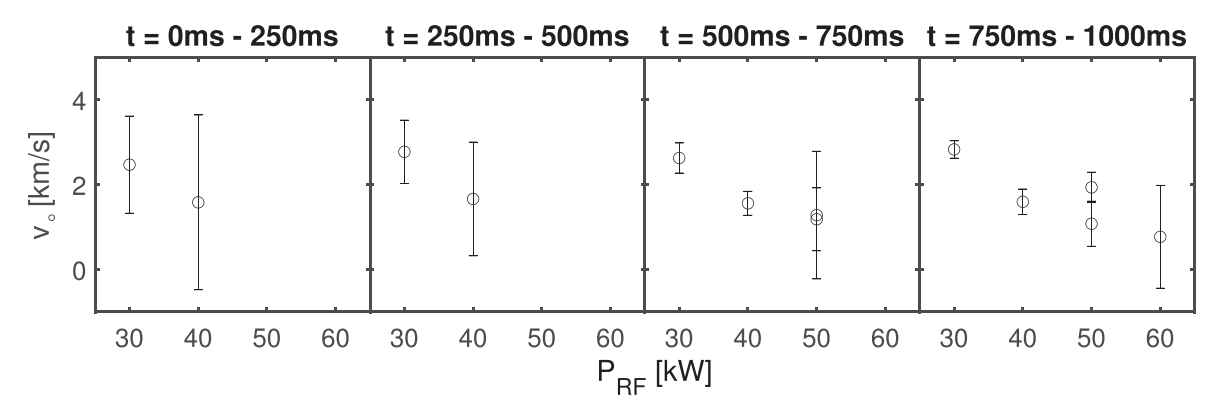


FIG. 7. Temporal evolution of neutral deuterium velocity as a function of power. Local bulk flow is observed to be radially inward and decreases monotonically as rf power increases. Neutral velocity is measured to be constant in time for a given rf power.

flat across the radius of Proto-MPEX. Absolute atomic densities derived from xenon and krypton are in excellent agreement. For a unique radial location, the absolute atomic density generally increases with time, as is expected since the gas pressure is increasing over the entirety of the plasma pulse.

Figure 10 shows the evolution of deuterium neutral temperature throughout the plasma pulse as a function of radial location. Temperatures, again, are measured to be approximately 0.2 eV. Neutral temperature shows no observable dependence over the radius of Proto-MPEX for these operating conditions. A general decrease in neutral temperature for a given radial location is measured throughout the plasma pulse.

The neutral atoms are measured to be moving radially inward at all radii investigated in this work, as shown in Fig. 11. The neutral bulk flow at each radial location is constant in time throughout the plasma pulse. The flow increases with radius near the axis of the plasma but is constant at the outer edge, r=6-7 cm, of the plasma. Non-zero flow is observed at r=0 likely due to increased absorption along the injected laser path, creating a larger spatial footprint that averages over a larger collection volume than intended.

#### V. DISCUSSION

Neutral deuterium velocity distributions were obtained as a function of time and radial location in Proto-MPEX fusion-relevant plasmas with the diagnostic situated  $\sim$ 20 m away from the device. Evolution of neutral atomic deuterium TALIF signal over a onesecond Proto-MPEX plasma pulse was measured with a resolution of 250 ms for different injected rf powers and radial locations. Discernible deuterium signal was observed for  $P_{\rm rf} = 30$ –60 kW. For early times in the plasma pulse, the TALIF SNR is very low or zero and increases over the plasma pulse duration, i.e., as the operating pressure increased the SNR increased. Neutral deuterium measurements were calibrated with both xenon and krypton static-fill reference cases. Absolute densities derived from both calibration gases show excellent agreement, making xenon a suitable replacement calibration gas for deuterium and eliminating the need to realign between target and calibration TALIF measurements. However, due to the poor SNR and added difficulty of obtaining suitable xenon NVDFs, it is recommended that krypton be used for deuterium calibration for ease of measurement.

The absolute atomic deuterium density shows no observable dependence on injected rf power or radial location for these operating conditions. However, atomic deuterium density generally increases over the plasma pulse. The increase in atomic deuterium density as a function of time is consistent with the increase in operating pressure over the plasma pulse. Approximate atomic deuterium densities are  ${\sim}10^{20} m^{-3}$  in Proto-MPEX. For these measurements and particular configuration of laser injection and collection, the minimum detectable density is  $\sim 1.8 \times 10^{20} \text{m}^{-3}$ . However, this lower limit is expected to decrease with longer data acquisition. Proto-MPEX was modeled for different operating conditions for different experiments using SOLPS. 25-27 For standard operation of Proto-MPEX for high density plasma experiments, i.e.,  $n_e \ge 6 \times 10^{19} m^{-3}$ , SOLPS predicts atomic neutral deuterium atomic densities of  $\sim 2 \times 10^{19} \mathrm{m}^{-3}$ . However, the operating pressure for the high density simulation is less than the operating pressures in this work. Additionally, simulated atomic neutral densities in the region of TALIF measurements are line averaged, likely underestimating local density values. Measured atomic densities reported here are in approximate agreement with predicted values from Ref. 27.

The neutral atomic deuterium temperature shows no observable dependence on injected rf power or radial location for these Proto-MPEX operational parameters. Neutral temperature was nominally measured to be 0.2 eV and generally decreased over the plasma pulse. Since the operating pressure increased rapidly over the plasma pulse, the plasma became more collisional and started to terminate for later times, both processes should result in a decrease in the neutral temperature over the duration of the plasma pulse. Owen *et al.* predicted molecular deuterium temperature in Proto-MPEX for standard operating conditions.  $^{26}$  The neutral molecular temperature predicted at the edge of the plasma, i.e., r=6-7 cm off mechanical axis for the experiments reported here, is 0.13 eV, slightly higher than the wall temperature for the simulation of 0.1 eV. While the measurements presented here are for atomic deuterium, the measured atomic and predicted molecular neutral temperatures are comparable.  $^{26}$ 

Local neutral bulk flow is constant for a unique injected rf power or radial location throughout the duration of the plasma pulse. Radial flow decreases for increasing injected rf power, likely due to increased ionization at higher rf powers. Neutral flow also increases for increasing radii until the plasma edge, and peak radial flows are ~3 km/s.

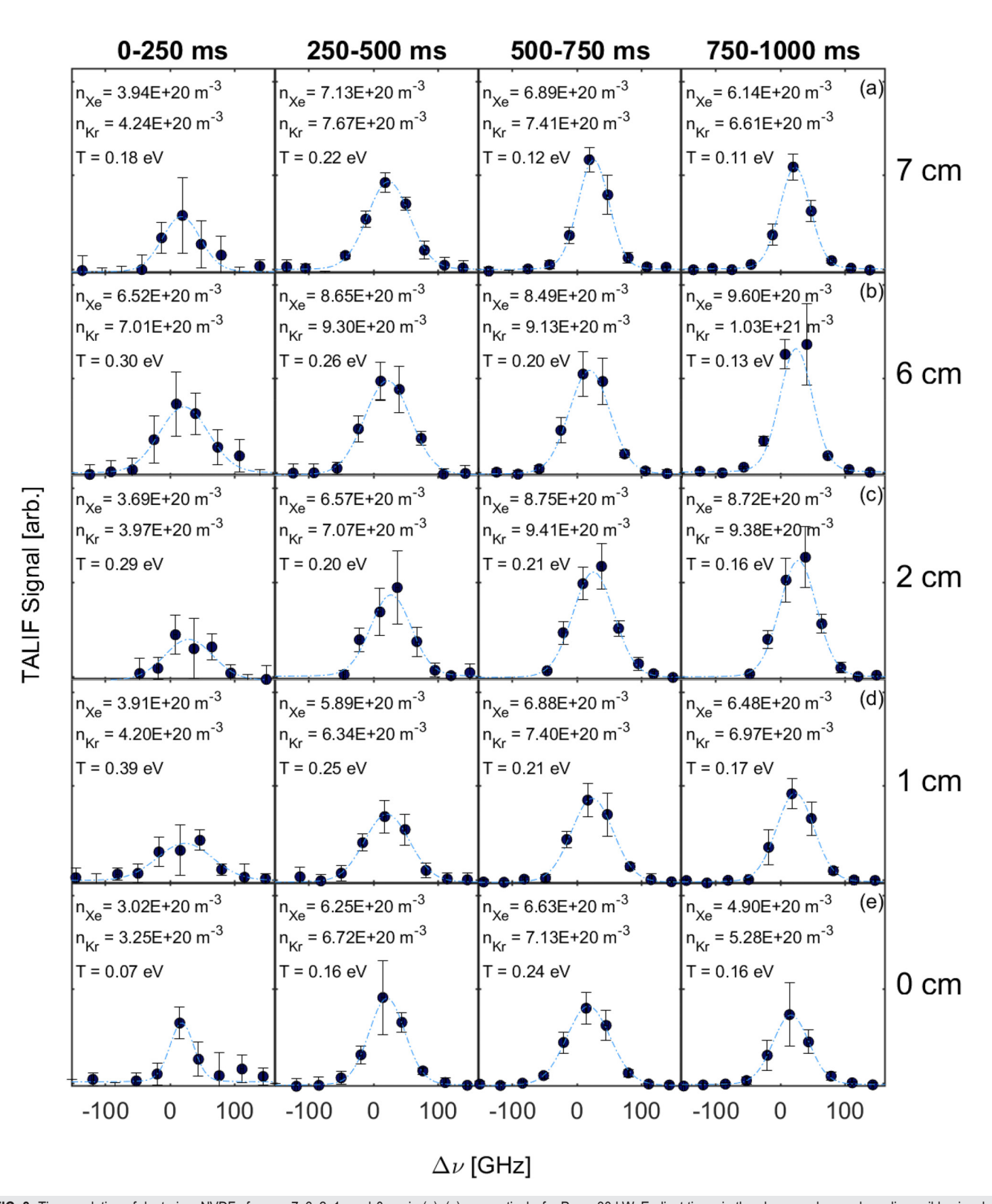


**FIG. 8.** Time evolution of deuterium NVDFs for r=7,6,2,1, and 0 cm in (a)–(e), respectively, for  $P_{\rm rf}=30$  kW. Earliest times in the plasma pulse produce discernible signal, but with low SNR which yields a large spread in signal as compared to later times.

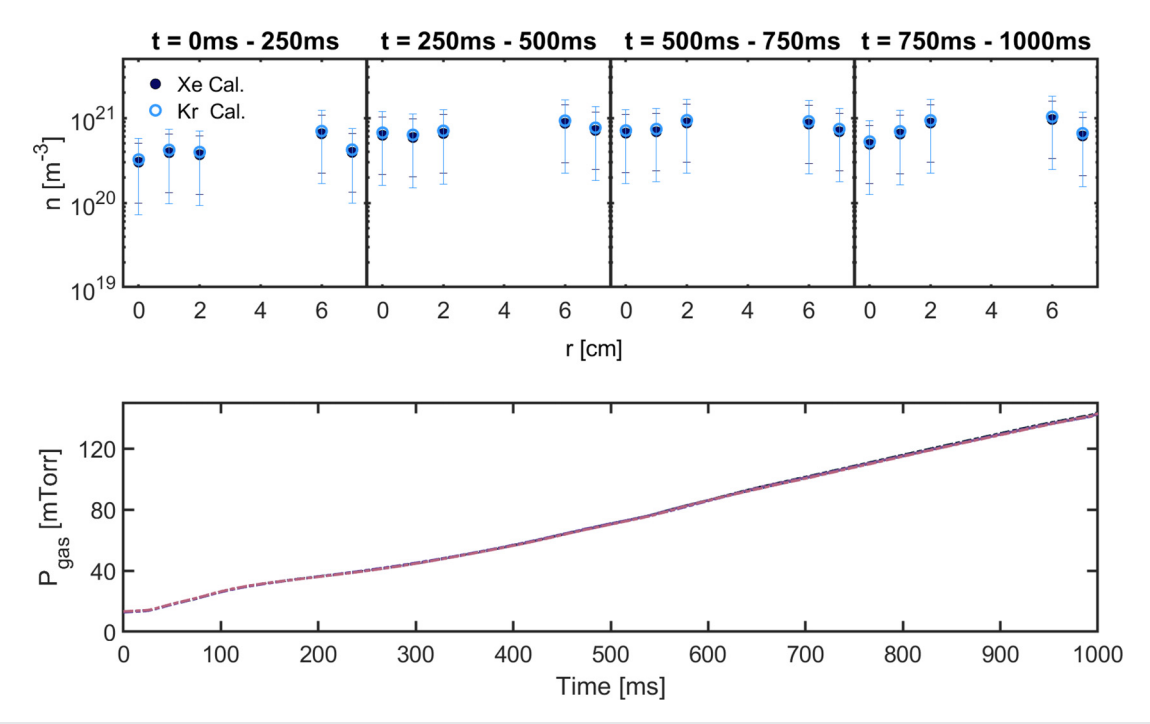


**FIG. 9.** (Upper) Evolution of atomic density vs r calibrated with both xenon (dark blue solid circles) and krypton (light blue open circles). Within the uncertainty of the measurement, the radial profile is essentially flat. Data for r = 3, 4, and 5 cm were inaccessible due to a magnetic support rod that physically obstructed the collection apparatus. (Lower) Evolution of total neutral pressure throughout the plasma pulse. All pressure traces for each radial location are plotted.

Significant inward radial neutral flow is measured in these experiments. There are likely several mechanisms that accelerate the neutrals to approximate their thermal velocities (~3 km/s). The most likely explanation for the observed inward radial neutral flows is charge exchange collisions with flowing ions. Possible mechanisms are discussed below in no particular order of dominance. Significant ionneutral coupling is expected given previous estimates of significant power losses in helicon plasmas due to ion-neutral charge exchange.<sup>28</sup>

Previous studies in Proto-MPEX using Mach probes reported parallel ion flows away from the antenna (toward the upstream boundary of the device) of  $\sim \! 10$  km/s.  $^{29}$  As the ions traverse the

TALIF measurement region, they experience a rapidly increasing magnetic field and the strongly magnetized ions are pinched by the converging magnetic field, imparting a large radial velocity to the ions. The magnetic field angle in the TALIF measurement region is determined from the ratio of the radial to axial magnetic field magnitudes. The projection of the ion flow along the convergent magnetic field provides an estimate of the likely radial ion flow. For the magnetic field geometry in this work, ions at the TALIF measurement location should have a radial velocity that is up to  $\sim\!10\%$  the parallel velocity. The magnetic component ratio is larger for larger radii in the plasma, implying a larger ion radial velocity for locations off axis, in agreement

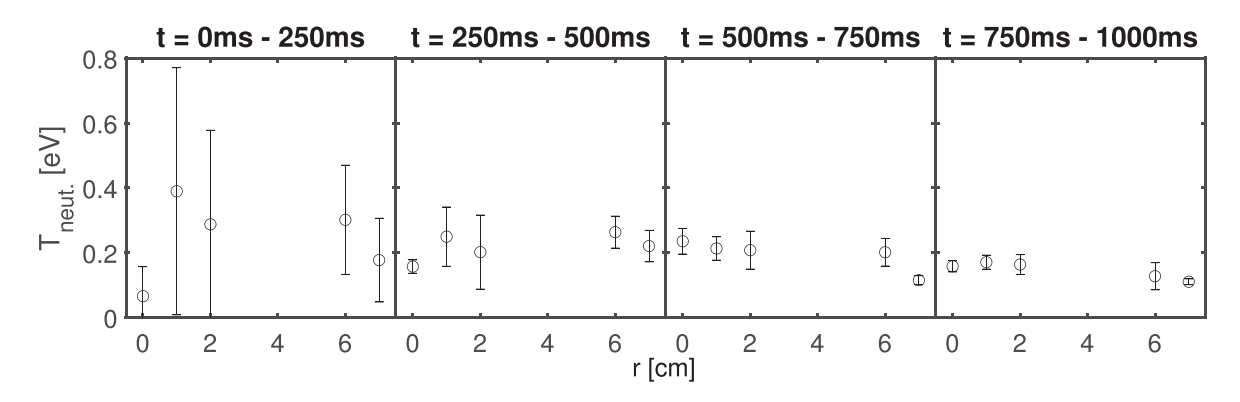


**FIG. 10.** Temperature vs *r* throughout the plasma pulse. Earliest times show large variation in neutral temperature that relaxes for later times. The temperature is only weakly dependent on radius but has a modest dependence on time. Neutral temperature decreases over the plasma pulse.

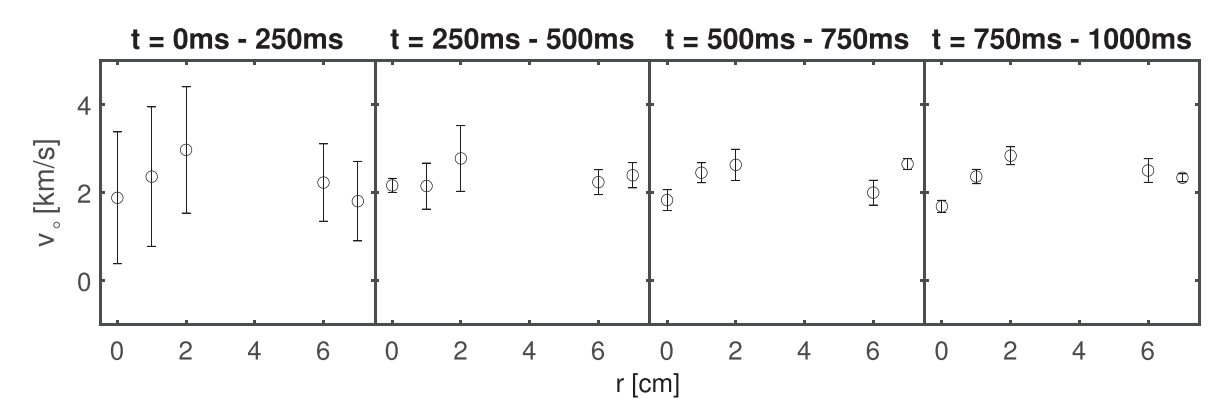


**FIG. 11.** Evolution of neutral velocity vs r throughout the plasma pulse. Earliest times show large variation in neutral bulk flow that relaxes for later times. The neutral motion is measured to be radially inward. Neutral velocity is constant for a fixed radial location but increases for increasing radius before asymptoting at the plasma edge (r = 6-7 cm).

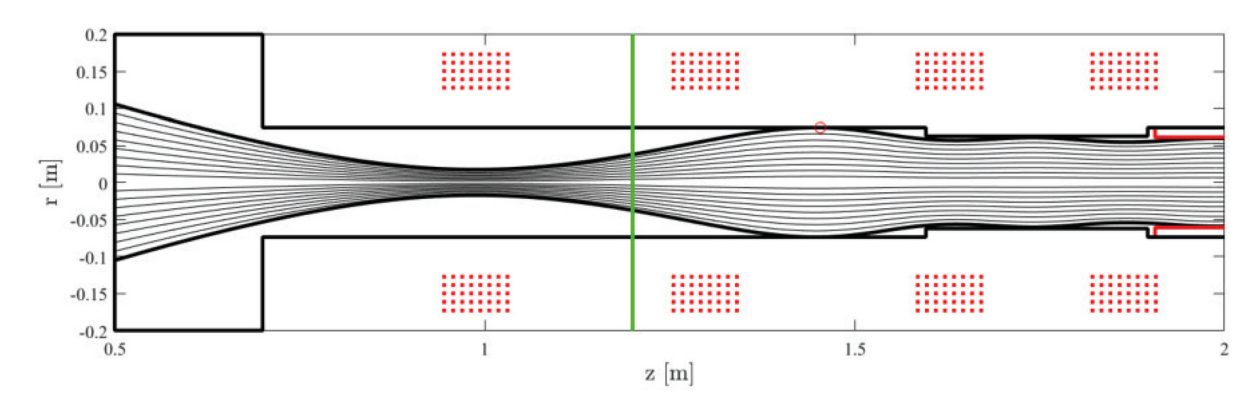


FIG. 12. Magnetic field geometry for the experiments presented in this work. A green vertical line indicates the TALIF measurement location. The ratio of radial and axial magnetic field components was calculated at different radial locations at the TALIF measurement region to provide an estimate of the ion radial velocity.

with the measured neutral flow. Figure 12 shows the magnetic field geometry upstream of the helicon antenna in Proto-MPEX, and a green line indicates the location of TALIF measurements. Through charge exchange collisions with the radially pinching ions, neutrals should pickup significant, inward, radial flow.

A second possible mechanism that likely contributes to the large measured radial neutral flow is particle flux balance. Hollow neutral profiles are common in helicon plasma sources, thus there is a radial gradient in neutral pressure.  $^{24}$  The large parallel ion flows away from the antenna region necessitate an inward flux of ions (or neutrals) to supply new ions to sustain the plasma. The escaping ions travel along the magnetic field that terminates on the dump chamber at the end of the device. Similar neutral inward radial flow is observed in the MARIA helicon plasma source for a uniform axial magnetic field, where neutral flows are measured to be  $\sim 20\%$  the thermal velocity and are believed to provide the needed fueling along the axis of the machine at locations throughout the plasma.  $^{30}$ 

Yet another possible explanation for the radial flows measured here is the possibility of contributions from azimuthal flows. The TALIF measures velocity components parallel to the injection axis of the laser beam and is agnostic to the system coordinate system. That is, a small optical misalignment or shift of the plasma column with respect to mechanical center of Proto-MPEX can introduce velocity components that are not purely coordinate-system radial. Azimuthal flows have been observed in helicon plasmas and could provide an azimuthal velocity to neutrals through charge exchange collisions. However, considerable care was taken to prevent misalignment of the confocal apparatus. While unlikely, it is possible that if the plasma columns are shifted from the device axis, some of the radial neutral flows could actually be an azimuthal flow component that is mis-identified. It is likely the neutral bulk flow reported in this work is a result of many or all of these processes and not one dominant mechanism. Assuming significant charge exchange interactions occur, these measurements provide indirect information about the ion motion in these regions.

# **ACKNOWLEDGMENTS**

The authors would like to thank Cuyler Beatty for helpful conversations and the Proto-MPEX team for assisting in these experiments. This work was supported by U.S. Department of Energy Grant Nos. DE-SC0017577 and DE-AC05-00OR22725. This

paper has been authored by UT-Battelle, LLC, under Contract No. DE-AC05-00OR22725 with the U.S. Department of Energy (DOE). The U.S. government retains and the publisher, by accepting the article for publication, acknowledges that the U.S. government retains a nonexclusive, paid-up, irrevocable, worldwide license to publish or reproduce the published form of this manuscript, or allow others to do so, for U.S. government purposes. DOE will provide public access to these results of federally sponsored research in accordance with the DOE Public Access Plan (http://energy.gov/downloads/doe-public-access-plan).

#### **DATA AVAILABILITY**

The data that support the findings of this study are available from the corresponding author upon reasonable request.

#### **REFERENCES**

- <sup>1</sup>E. Marmar, "Recycling processes in tokamaks," J. Nucl. Mater. **76-77**, 59–67 (1978).
- <sup>2</sup>R. Hazeltine, M. Calvin, P. Valanju, and E. Solano, "Analytical calculation of neutral transport and its effect on ions," Nucl. Fusion 32, 3–14 (1992).
- <sup>3</sup>R. L. Boivin, J. A. Goetz, A. E. Hubbard, J. W. Hughes, I. H. Hutchinson, J. H. Irby, B. LaBombard, E. S. Marmar, D. Mossessian, C. S. Pitcher, J. L. Terry, B. A. Carreras, and L. W. Owen, "Effects of neutral particles on edge dynamics in Alcator C-Mod plasmas," Phys. Plasmas 7, 1919–1926 (2000).
- <sup>4</sup>L. Chen, G. Xu, A. Nielsen, W. Gao, Y. Duan, H. Liu, L. Wang, M. Li, M. Wang, X. Zhang, R. Chen, H. Wang, Z. Sun, S. Ding, N. Yan, S. Liu, L. Shao, W. Zhang, G. Hu, J. Li, L. Zhang, and B. Wan, "Study on the L–H transition power threshold with RF heating and lithium-wall coating on EAST," Nucl. Fusion 56, 056013 (2016).
- <sup>5</sup>P. Snyder, J. Hughes, T. Osborne, C. Paz-Soldan, W. Solomon, M. Knolker, D. Eldon, T. Evans, T. Golfinopoulos, B. Grierson, R. Groebner, A. Hubbard, E. Kolemen, B. LaBombard, F. Laggner, O. Meneghini, S. Mordijck, T. Petrie, S. Scott, H. Wang, H. Wilson, and Y. Zhu, "High fusion performance in super H-mode experiments on Alcator C-Mod and DIII-D," Nucl. Fusion 59, 086017 (2019).
- <sup>6</sup>P. Mertens and M. Silz, "Radial profiles of atomic deuterium measured in the boundary of TEXTOR 94 with laser-induced fluorescence," J. Nucl. Mater. **241-243**, 842–847 (1997).
- <sup>7</sup>R. Schneider, X. Bonnin, K. Borrass, D. P. Coster, H. Kastelewicz, D. Reiter, V. A. Rozhansky, and B. J. Braams, "Plasma edge physics with B2-Eirene," Contrib. Plasma Phys. 46, 3–191 (2006).
- <sup>8</sup>A. E. Hubbard, "Physics and scaling of the H-mode pedestal," Plasma Phys. Controlled Fusion 42, A15–A35 (2000).
- <sup>9</sup>J. W. Connor and H. R. Wilson, "A review of theories of the L-H transition," Plasma Phys. Controlled Fusion **42**, R1–R74 (1999).
- <sup>10</sup>R. A. Stern and J. A. Johnson, "Plasma ion diagnostics using resonant fluorescence," Phys. Rev. Lett. 34, 1548–1551 (1975).
- <sup>11</sup>S. Mazouffre, C. Foissac, P. Supiot, P. Vankan, R. Engeln, D. Schram, and N. Sadeghi, "Density and temperature in n atoms in the afterglow of a microwave discharge measured by two-photon laser-induced fluorescence technique," Plasma Sources Sci. Technol. 10, 168–175 (2001).
- <sup>12</sup>H. Döbele, T. Mosbach, K. Niemi, and V. Schulz-von der Gathen, "Laser-induced fluorescence measurements of absolute atomic densities: Concepts and limitations," Plasma Sources Sci. Technol. 14, S31–S41 (2005).
- <sup>13</sup>E. Es-sebbar, Y. Benilan, A. Jolly, and M.-C. Gazzeau, "Characterization of an N2 flowing microwave post-discharge by OES spectroscopy and determination of absolute ground-state nitrogen atom densities by TALIF," J. Phys. D: Appl. Phys. 42, 135206 (2009).
- <sup>14</sup>K. Niemi, V. S. von der Gathen, and H. F. D. obele, "Absolute atomic oxygen density measurements by two-photon absorption laser-induced fluorescence

- spectroscopy in an RF-excited atmospheric pressure plasma jet," Plasma Sources Sci. Technol. 14, 375–386 (2005).
- <sup>15</sup>T. Kajiwara, T. Shinkawa, K. Uchino, M. Masuda, K. Muraoka, T. Okada, M. Maeda, S. Sudo, and T. Obiki, "Application of two-photon-excited laser-induced fluorescence to atomic hydrogen measurements in the edge region of high-temperature plasmas," Rev. Sci. Instrum. 62, 2345–2349 (1991).
- <sup>16</sup>D. Elliott, D. Sutherland, U. Siddiqui, E. Scime, C. Everson, K. Morgan, A. Hossack, B. Nelson, and T. Jarboe, "Two-photon LIF on the HIT-SI3 experiment: Absolute density and temperature measurements of deuterium neutrals," Rev. Sci. Instrum. 87, 11E506 (2016).
- <sup>17</sup>D. Elliot, E. Scime, and Z. Short, "Novel calibration scheme for two-photon absorption laser induced fluorescence of hydrogen," Rev. Sci. Instrum. 87, 11E504 (2016).
- <sup>18</sup>J. B. O. Caughman, R. H. Goulding, T. M. Biewer, T. S. Bigelow, I. H. Campbell, J. Caneses, S. J. Diem, A. Fadnek, D. T. Fehling, R. C. Isler, E. H. Martin, C. M. Parish, J. Rapp, K. Wang, C. J. Beers, D. Donovan, N. Kafle, H. B. Ray, G. C. Shaw, and M. A. Showers, "Plasma source development for fusion-relevant material testing," J. Vac. Sci. Technol. A 35, 03E114 (2017).
- <sup>19</sup>J. Rapp, A. Lumsdaine, C. Beers, T. Biewer, T. M. Bigelow, J. Caneses, J. Caughman, R. Goulding, N. Kafle, C. Lau, E. Lindquist, P. Piotrowicz, H. Ray, and M. Showers, and the MPEX Team. "Latest results from Proto-MPEX and the future plans for MPEX," Fusion Sci. Technol. 75, 654–663 (2019).
- 20 S. Hiroe, R. Colchin, G. Haste, F. Baity, D. Bates, L. Berry, T. Bigelow, R. Burris, J. Cobble, W. Davis, R. Donaldson, J. Glowienka, D. Hillis, H. Kimrey, R. Livesey, J. Mankin, M. McGuffin, D. Overbey, B. Peterson, D. Rasmussen, R. Richards, C. Schaich, G. Sullivan, D. Swain, T. Uckan, T. White, J. Wilgen, R. Wintenberg, K. Young, K. Connor, J. Goyer, R. Hickok, L. Solensten, F. Bieniosek, R. Juhala, T. Owens, D. Boyd, R. Mahon, V. Yun, B. Quon, Jaycor, O. Hankins, W. Casson, and K. Carpenter, "Summary of ELMO bumpy torus (EBT-S) experiments from 1982 to 1984," Nucl. Fusion 28, 2249–2263 (1988).
- <sup>21</sup>R. Loudon, *The Quantum Theory of Light*, 2nd ed. (Clarendon Press, New York, 1983).
- <sup>22</sup>K. Niemi, V. Schulz-von der Gathen, and H. Dbele, "Absolute calibration of atomic density measurements by laser-induced fluorescence spectroscopy with two-photon excitation," J. Phys. D: Appl. Phys. 34, 2330–2335 (2001).
- <sup>23</sup>R. Janev, W. Langer, K. Evans, Jr., and D. Post, Jr., Elementary Processes in Hydrogen-Helium Plasmas, 1st ed. (Springer, 1987) p. 44.
- 24 M. Galante, R. Magee, and E. Scime, "Two-photon laser induced fluorescence measurements of neutral density in a helicon plasma," Phys. Plasmas 21, 055704 (2014).
- <sup>25</sup>J. Rapp, L. Owen, X. Bonnin, J. Caneses, J. Canik, C. Corr, and J. Lore, "Transport simulations of linear plasma generators with the B2.5-Eirene and EMC3-Eirene codes," J. Nucl. Mater. 463, 510–514 (2015).
- <sup>26</sup>L. W. Owen, J. Rapp, J. Canik, and J. D. Lore, "Transport modeling of convection dominated helicon discharges in Proto-MPEX with the B2.5-Eirene code," Phys. Plasmas 24, 112504 (2017).
- <sup>27</sup>J. Rapp, L. W. Owen, J. Canik, J. D. Lore, J. F. Caneses, N. Kafle, H. Ray, and M. Showers, "Radial transport modeling of high density deuterium plasmas in Proto-MPEX with the B2.5-Eirene code," Phys. Plasmas 26, 042513 (2019).
- 28S. C. Thakur, M. Paul, E. M. Hollman, E. Lister, E. Scime, S. Sadhu, T. Steinberger, and G. Tynan, "Ion heating in the PISCES-Rf liquid-cooled high-power, steady-state, helicon plasma device," Plasma Sources Sci. Technol. (to be published) (2021).
- <sup>29</sup>N. Kafle, L. W. Owen, J. F. Caneses, T. M. Biewer, J. B. O. Caughman, D. C. Donovan, R. H. Goulding, and J. Rapp, "Plasma flow measurements in the prototype-material plasma exposure experiment (Proto-MPEX) and comparison with B2.5-Eirene modeling," Phys. Plasmas 25, 052508 (2018).
- 30J. Green, O. Schmitz, and M. Zepp, "Direct measurement of the ionization source rate and closure of the particle balance in a helicon plasma using laser induced fluorescence," Phys. Plasmas 27, 043511 (2020).
- <sup>51</sup>E. Scime, R. Hardin, C. Biloiu, A. M. Keesee, and X. Sun, "Flow, flow shear, and related profiles in helicon plasmas," Phys. Plasmas 14, 043505 (2007).